Check for updates

Electrolysis of ethylene to ethylene glycol paired with acidic CO_2-to-CO conversion

Hongjun Chen,†*[abd] Heejong Shin,†‡[cd] Jianan Erick Huang,†[cd] Hengzhou Liu, [ID][cd] Rui Kai Miao,[e] Rong Xia,[cd] Weiyan Ni,[cd] Jiaqi Yu,[cd] Yongxiang Liang,[cd] Bosi Peng,[cd] Yuanjun Chen,[cd] Guangcan Su, [ID][cd] Ke Xie,*[cd] Anita Ho-Baillie [ID]*[ab] and Edward H. Sargent [ID]*[cd]

Electrochemical conversion of CO_2 into CO, ethylene, and other valuable chemicals is a promising method for carbon capture and utilisation. However, when carried out in an alkaline or neutral media, (bi)carbonate formation leads to low atom efficiency in the electrocatalytic process. In contrast, acidic conditions enable >80% CO_2 utilization, but there is a need to lower full-cell voltage. In this work, we paired the acidic cathodic CO_2-to-CO reaction with acidic anodic ethylene-to-ethylene glycol (C_2H_4-to-EG) conversion for the first time. For the selective oxidation of ethylene to EG, we employed a homogeneous redox mediator ruthenium–polyoxometalate (Ru–POM) with gold-modified electrodes for the first time to facilitate the redox cycle. This resulted in enhanced selectivity and stability, achieving a faradaic efficiency (FE) of 83% for EG. At the cathode, a porous nickel single-atom catalyst drives the conversion of CO_2 into CO in an acidic electrolyte with an FE of 97%. The paired system operates at a full-cell voltage of 3.1 V, compared to 3.3 V for a reference system using the oxygen evolution reaction. The demonstrated system offers a promising route for reducing carbon emissions with high atom efficiency.

Broader context

Electrochemical CO_2 conversion to CO, ethylene, and other valuable chemicals is a promising route to reduce carbon emissions. However, in alkaline or neutral media, over 85% of CO_2 is lost to carbonate formation, while acidic systems suffer from an inefficient and energy-intensive oxygen evolution reaction (OER) at the anode. Moreover, O_2 as a byproduct holds little economic value (∼$25 per ton), limiting overall viability. To address these challenges, we pair CO_2 reduction with ethylene oxidation to ethylene glycol (EG) using a Ru-based polyoxometalate (Ru–POM) redox mediator. This strategy upgrades ethylene—a key CO_2 reduction product—into EG, a high-value industrial chemical used in polyesters, resins, and antifreezing. Compared to the traditional EG production process, which emits ∼1.6 tonnes of CO_2 per tonne of EG, this method offers a low-emission alternative. Our approach combines CO_2 utilization with value-added anodic chemistry, enhancing energy efficiency and economic potential. This work is relevant to researchers in electrocatalysis, green chemistry, and industrial decarbonization.

[a] School of Physics, Faculty of Science, The University of Sydney, Sydney, NSW 2006, Australia. E-mail: hongjun.chen@sydney.edu.au, anita.ho-baillie@sydney.edu.au

[b] The University of Sydney Nano Institute, The University of Sydney, Sydney, NSW 2006, Australia

[c] Department of Chemistry, Northwestern University, Evanston, Illinois, 60208, USA. E-mail: ke-xie@northwestern.edu, ted.sargent@northwestern.edu

[d] Department of Electrical and Computer Engineering, Northwestern University, Evanston, Illinois, 60208, USA

[e] Department of Mechanical and Industrial Engineering, University of Toronto, Toronto, Ontario, Canada

† These authors contributed equally.

‡ Present address: Department of Chemical and Biomolecular Engineering, Sogang University, Seoul 04107, Republic of Korea.
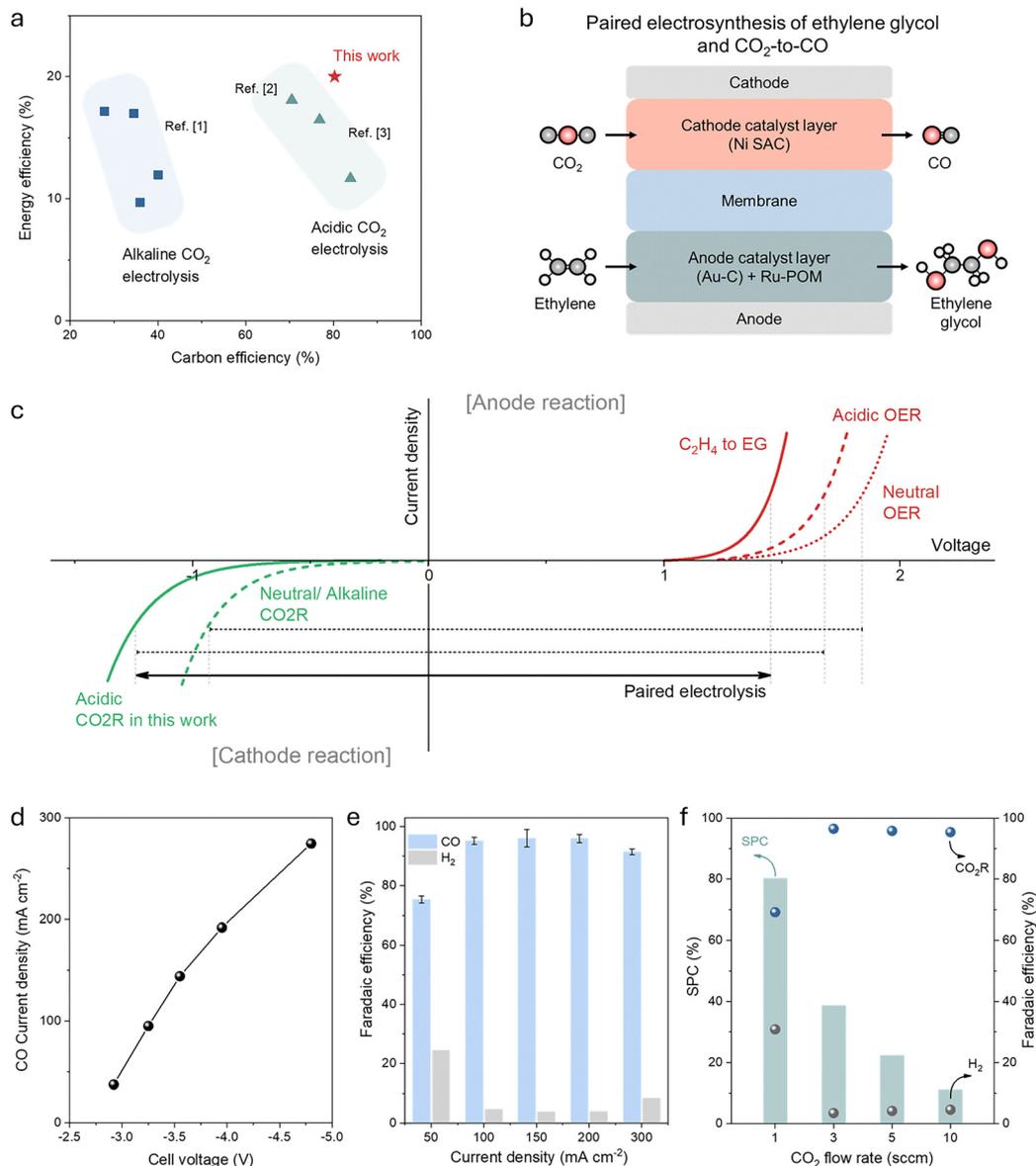
1. Introduction

Electrochemical CO_2 reduction (CO_2R) to valuable chemicals such as CO, ethylene and ethanol is a promising means to reduce carbon intensity.[1] However, when conducted in an alkaline or neutral environment, a majority of CO_2 is lost to (bi)carbonate formation. To address this issue, acidic CO_2R methods have been developed, enabling single-pass CO_2 conversion efficiency, which is the percentage of CO_2 converted relative to the total input, to exceed 80%.[2–6] These acidic systems typically require ∼4 V to deliver 200 mA cm^{-2} when paired with the kinetically limiting oxygen evolution reaction (OER) (Fig. 1a).[7–9]

8600 | *Energy Environ. Sci.*, 2025, **18**, 8600–8607

This journal is © The Royal Society of Chemistry 2025

Fig. 1 (a) Energy efficiency vs carbon efficiency of alkaline (square) and acidic (triangle) CO_2-to-CO conversions. Value achieved by this work is represented by the star symbol. (b) Schematic of the acidic CO_2-to-CO conversion paired with ethylene-to-ethylene glycol electrolysis. (c) Qualitative performance comparisons of neutral and acidic reactions for unpaired and paired CO_2 to CO conversions. (d) Cell voltages required for acidic CO_2-to-CO conversion (0.05 M H_2SO_4 – 2.5 M KCl) at different current densities. (e) Faradaic efficiency for CO and H_2 on a nickel single-atom catalyst (NiSAC). (f) Single-pass CO_2 conversion SPC efficiency (left Y-axis) and FE (right Y-axis) as a function of CO_2 flow rates.

Pairing CO_2R with alternative electrochemical processes presents an opportunity to increase the total kg of CO_2 abated per kWh of electricity.[7,10,11] Since O_2 gas is abundant with limited economic value, it is desirable to develop alternative electrochemical processes to replace the OER to increase the overall reaction profit. The production of ethylene glycol (EG) from ethylene is of particular interest since it has an annual demand of 20 million tonnes.[12–15] Today, the production of EG follows a two-step thermocatalytic process: ethylene (C_2H_4) is first epoxidized to ethylene oxide (EO) under high pressure and temperature, followed by EO hydrolysis in the presence of a strong acid. This leads to ∼1.6 tonnes of CO_2 per tonne of EG.[16]

Electrochemical production of EG from C_2H_4 is a promising alternative that could potentially improve the overall profit of the full cell and reduce the carbon intensity if achieved efficiently under mild reaction conditions, in light of its high industrial value and carbon intensity. In addition, the low thermodynamic potential for ethylene oxidation (0.6 V *vs.* standard hydrogen electrode (SHE)) is expected to further reduce full cell voltage compared to the traditional OER process (1.23 V *vs.* SHE). Furthermore, a chemical loop is potentially built if C_2H_4 is the main product generated from CO_2R or electrochemical CO reduction (COR) after further improvement on product selectivity and efficiency in the near future.

Successful demonstration includes the use of electrochemically generated hypochlorous acid (HClO), but the possibility of producing chlorinated organics is undesirable. Additionally, the high thermodynamic potential for the Cl evolution reaction (1.36 V *vs.* SHE) actually causes a higher full cell voltage, motivating the search for other options.[17–22] To date, the performance of a direct one-step electrochemical C_2H_4-to-EG conversion has been limited to $J_{partial} < 20$ mA cm^{-2} [23] and a faradaic efficiency (FE) of 60–90%.[15,23,24]

Here, we report a paired electrolysis system (Fig. 1b) that couples C_2H_4-to-EG conversion using a ruthenium–polyoxometalate (Ru–POM) redox mediator with an acidic CO_2-to-CO conversion with a porous nickel single-atom catalyst (NiSAC). The Ru–POM redox selectively oxidizes the C_2H_4-to-EG conversion with a FE of 83%, while the CO_2-to-CO conversion achieved a FE of 97%. The system operates at a full cell voltage of 3.1 V, compared with 3.3 V for acidic CO_2R paired with an acidic OER (Fig. 1c). We also developed a gold-modified carbon felt electrode to accelerate the Ru–POM redox cycle, thereby increasing EG productivity while protecting the carbon substrate underneath during anodic oxidation.

2. Results and discussion

To facilitate acidic CO_2-to-CO conversion, we developed NiSAC for the cathode, with atomically dispersed Ni sites serving as active centers for selective CO production from CO_2. To maximize the number of electrochemically accessible Ni active sites, a porous structure based on ~50 nm-sized Zeolite imidazolate frameworks-8 (ZIF-8) was employed,[25,26] an approach that addresses the limited accessibility of inner micropores. High-resolution transmission electron microscopy (HR-TEM) images and energy dispersive spectroscopy mapping showed the uniform dispersion of Ni sites on the carbon support (Fig. S1). Results from X-ray absorption spectroscopy (XAS) revealed that the Ni atoms remain atomically dispersed, with no metallic nickel or nickel oxide-based nanoparticles on the NiSAC (Fig. S2). Results from X-ray photoelectron spectroscopy (XPS) showed pyridinic nitrogen peaks in the N 1s spectra, indicating strong Ni–N bonding which is evidence for the presence of Ni atoms (Fig. S3).

We then evaluated acidic CO_2R performance in a flow-cell electrolyzer with a buffered acidic electrolyte composed of 2.5 M KCl in 0.05 M H_2SO_4 as the catholyte and 0.05 M H_2SO_4 as the anolyte. For the optimization of the acidic CO_2R performance, the cathodic CO_2R was paired with an acidic OER half-reaction using an IrO_x–Ti mesh anode. The current density was varied from 50 to 300 mA cm^{-2} in a slim flow cell, and the applied full cell voltage was also varied from 2.9 to 4.8 V (Fig. 1d). The NiSAC electrode produced CO with a FE of 97% at 100 mA cm^{-2} (Fig. 1e). The catalytic performance of NiSAC was consistent regardless of catalyst loading (from 0.6 to 2.3 mg cm^{-2}), maintaining a CO FE of over 95% (Fig. S4). We found that increasing the pH from 0.3 to 1.0 or even 1.7 promoted the CO FE from <60% to 97% (Fig. S5). Therefore, for subsequent experiments, a pH of 1.0 was chosen for the catholyte which was composed of 2.5 M KCl + 0.05 M H_2SO_4, where KCl offers cation effects to trigger CO_2 reduction.

Acidic electrolytes minimize carbonate formation, thus enabling increased carbon utilization compared to neutral and alkaline solutions (Fig. 1c). In principle, lowering the pH of the anolyte facilitates proton transport and addresses salt formation. However, the lower anolyte pH also decreases CO_2R FE due to the faster proton transport that leads to HER. We sought to balance CO_2R performance and salt formation at 100 mA cm^{-2} *via* the use of 0.05 M H_2SO_4. Under the optimized condition, this limited salt formation and retained CO FE at above 90%. Completely avoiding salt formation is an important area for future work.

Lowering the CO_2 flow rate from 10 to 1 standard cubic centimeters per minute (sccm) enabled us to increase the single-pass CO_2 conversion (SPC) to CO from 11% to 80% at 100 mA cm^{-2} (Fig. 1f). This is higher than that in alkaline and neutral CO_2-to-CO electrolyzers, which are typically limited to $< \sim 50\%$.[6,27–29]

We also studied the stability of NiSAC (Fig. S6). During an extended electrolysis at 100 mA cm^{-2}, the system maintained an FE to CO of 97% over 16 h, with a slight potential shift from −3.3 to −3.5 V. Results from scanning electron microscopy (SEM) and XPS of the NiSAC after 16 h of electrolysis showed negligible changes in the electrode surface morphology (Fig. S7) and composition (Fig. S3).

For the anode development, we considered both direct (Fig. 2a) and mediated (Fig. 2b) ethylene oxidation. In each case, the competing reaction is water oxidation to O_2. In direct oxidation, the goal must be to transfer the reactive oxygen intermediates associated with water oxidation – (*OH, *O, and *OOH) – over to C_2H_4 before these intermediates are fully oxidized to O_2. In this case, electrooxidation is initiated by electron transfer at the catalyst surface. The thermodynamic potential for the ethylene oxidation (0.6 V *vs.* SHE) is much lower than that for OER (1.23 V *vs.* SHE). However, the actual ethylene oxidation process requires surface oxygen intermediates from water oxidation, and the slow kinetics of ethylene oxidation leads to a much higher overpotential than OER under a similar current density.[15,23]

Under the redox-mediated approach, the Ru–POM strategy (Fig. S8) was developed whereby Ru–POM was oxidized to an electron-deficient species, Ru–POM*, by the anode. This, in turn, oxidized C_2H_4-to-EG with the recovery of Ru–POM (Fig. 2b).[30–33] The redox of POM also has a lower thermodynamic oxidation potential than the water oxidation,[34] as well as a faster kinetics than both ethylene oxidation and OER, which could decrease the actual full cell operating potential.

With OER as the competing reaction, it can be inferred that the catalyst with a high OER activity might result in a low FE for EG production. Therefore, we posited that the catalyst with a weaker O binding than the Pt group metals, with a higher redox potential than that of Ru–POM, can facilitate the oxidation of Ru–POM. To best protect the anode for Ru–POM oxidation in an acidic electrolyte, we herein designed a Au-modified carbon felt (Au/C) for the low activity of Au in OER. Compared to other anode materials such as bare carbon felt, Au-modified C-400,
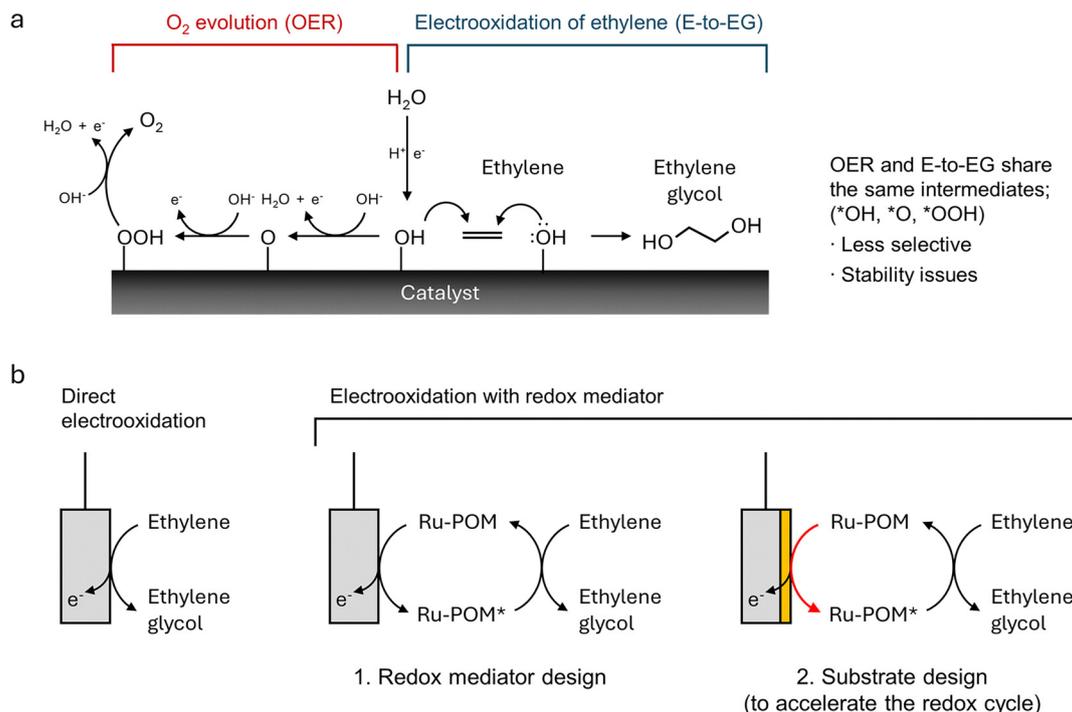
8602 | *Energy Environ. Sci.*, 2025, **18**, 8600–8607

This journal is © The Royal Society of Chemistry 2025

Fig. 2 (a) Ethylene oxidation pathways and the competition between ethylene and water oxidation for the oxygen intermediate species produced on the electrode under operating bias. These direct electrooxidation processes share the same intermediates (*OH, *O, and *OOH). (b) Electrooxidation of ethylene to EG *via* direct oxidation or using a redox mediator cycle (Ru–POM, the reduced state; Ru–POM*, the activated state).

noble metals Pt and Pd on carbon felts and metal oxides (CoO_x, RuO_x) on carbon felts, Au/C achieved the best performance, preferring Ru–POM activation over water oxidation (Fig. 3a). The highest FE was obtained when 0.1 M $HClO_4$ (Fig. S9) and 0.1 mM Ru–POM (Fig. S10) were used. The result in Fig. S10 also highlighted the importance of Ru–POM's presence, as FE $\sim$ 0% in the absence of Ru–POM.

To investigate the mechanism of the improved ethylene oxidation selectivity on the Au/C catalyst, we conducted cyclic voltammetry (CV) and linear sweep voltammetry (LSV) for Ru–POM mediated EG production to compare the performance of Au/C and C electrodes with and without a continuous ethylene supply (Fig. 3c), and with and without Ru–POM (Fig. 3d), respectively. Results showed that the anodic current increased beyond 1.2 V (*vs.* Ag/AgCl) when both Ru–POM and C_2H_4 were present, suggesting that the current increase is a result of C_2H_4 oxidation mediated by Ru–POM. The use of the Au/C electrode increased the current density by 1.5 times at 1.5 V (*vs.* Ag/AgCl) compared to the bare C electrode. Therefore, we can conclude that the Au layer was effective in activating the redox mediator at the electrode–electrolyte interfaces to drive the Ru–POM redox cycle. More importantly, a pair of redox peaks located around 0.9 V is more prominent on the Au/C electrode than that of the bare C electrode, indicating a fast kinetic reaction of Ru–POM in the presence of Au.

We hypothesize that Au produces an oxygen intermediate species that is slow to evolve to O_2, thereby enabling the intermediates to be carried by Ru–POM to oxidize C_2H_4 to EG (Fig. 3b). This cycle offers an alternative oxygen pathway, acting

as a redox mediator that is first oxidized at the electrode surface and then reduced back to Ru–POM.[35] This is confirmed by the results from *in situ* Raman spectroscopy of the Au/C electrode when operating at voltages from 1.1 V to 1.8 V in 0.1 M $HClO_4$, with (Fig. 3e) and without (Fig. 3f) Ru–POM. When Ru–POM was absent, the Au-O peak[36] (at 580 cm^{-1}) emerged when the voltage was increased to 1.4 V (Fig. 3g) and the peak intensity increased further with increasing voltage. In the presence of Ru–POM, the intensity of the Au-O peak was negligible for a wide voltage range (Fig. 3g). These results show evidence of Ru–POM instead of the Au oxidation when Ru–POM was present, suggesting that the oxygen intermediates formed on the Au surface were quickly consumed by Ru–POM instead of the occurrence of OER (Fig. 3b). This is also confirmed by the XPS results from the Au/C electrodes (Fig. S11). Therefore, Au/C accelerates the Ru–POM redox cycle, resulting in a modest improvement with a 6% increase in Fe compared to the bare carbon electrode.

In terms of the relationship between the cell voltage and E-to-EG partial current density (Fig. S12), as the cell voltage increased from 1.7 to 3.3 V, the E-to-EG partial current density first rose from 20 to 75 mA cm^{-2} at 2.3 V, and then declined to 30 mA cm^{-2} at 3.3 V. This is likely due to OER competition and EG decomposition at higher voltages (Fig. S13). The latter is more likely to proceed when the C electrode is used compared to the Au/C electrode. The better relative stability of the Au/C electrode can be seen in Fig. 4a and Fig. S14, showing higher FE retention after 1 hour of operation and stable voltage for 6000 seconds (1.6 hours) when the Au/C electrode is used compared to the carbon electrode, which degrades, requiring regular replacements (Fig. 4a).
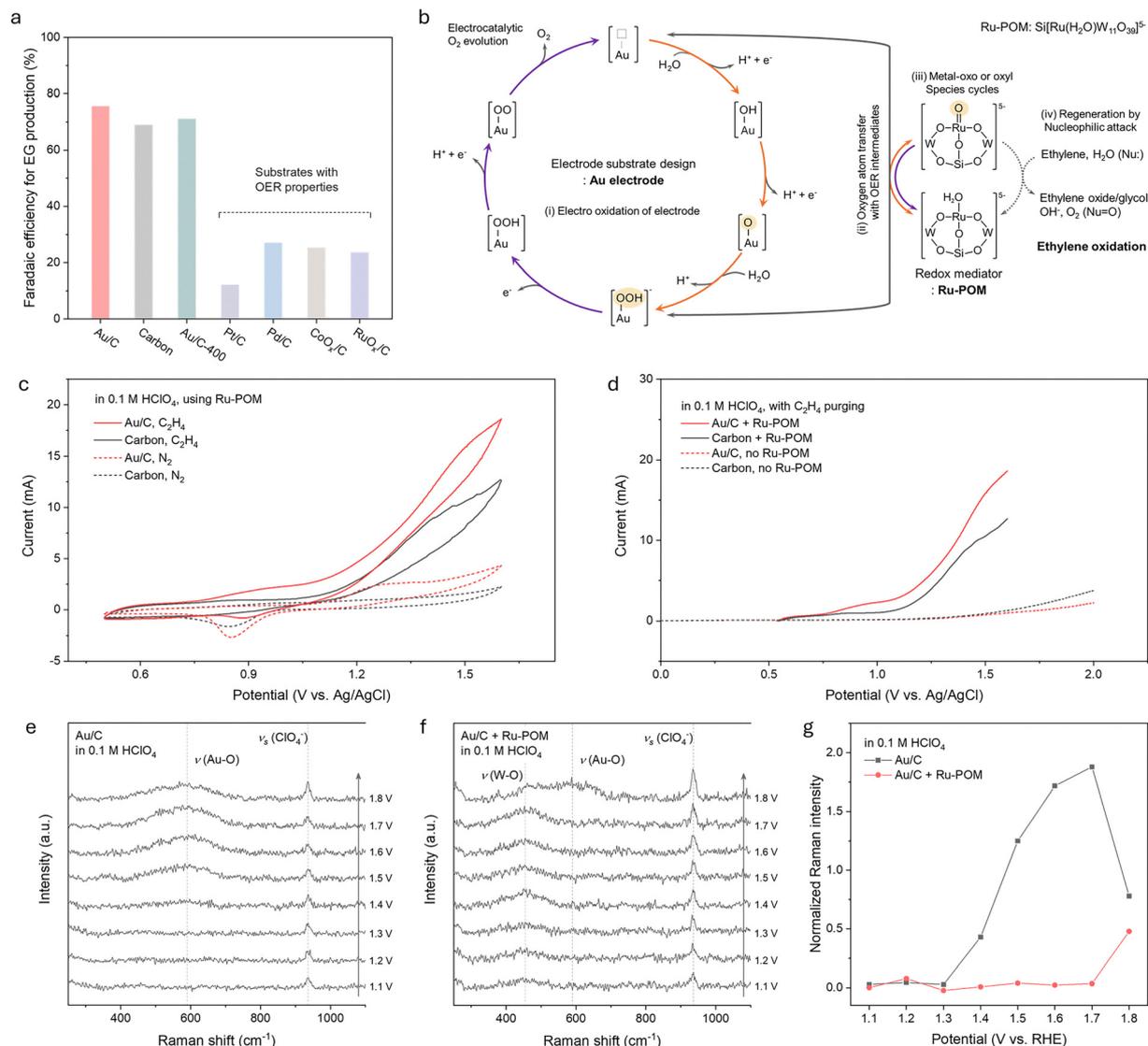
Fig. 3 (a) Comparison of FE for EG production using various electrode materials. (b) Schematic of a new pathway involving oxygen atom transfer between the oxygen intermediate species at Au sites and the Ru–POM redox cycle. (c) Cyclic voltammetry (CV) curves of EG production with Au/C (red) or carbon (black) electrodes in 0.1 M HClO$_4$ with (solid lines) and without (dashed lines) a continuous ethylene supply. (d) Linear sweep voltammetry (LSV) curves of EG production with Au/C (red) or carbon (black) electrodes with (solid lines) and without (dashed lines) Ru–POM mediators in 0.1 M HClO$_4$ with continuous C$_2$H$_4$ supply. Pt sheet and Ag/AgCl (saturated KCl) electrode were used as the counter and reference electrodes, respectively. *In situ* Raman spectra of the electrooxidation on the Au/C electrode surface in 0.1 M HClO$_4$ (e) without and (f) with 0.1 M Ru–POM. (g) Normalized Raman intensities of the AuO stretching mode from (e) and (f). The E-to-EG reaction paired with the hydrogen evolution reaction (HER) in (a), (c) to (g). (a) is a two-electrode system, while the rest are three-electrode systems.

The stability of the paired system that combines anodic C$_2$H$_4$-to-EG conversion with the cathodic acidic CO$_2$-to-CO reaction is shown in Fig. 4b. Over the course of 2 hours of electrolysis, the FE for CO production remained above 95%, and the FE for EG production remained above 80%. Another advantage of the EG pairing is the lower full cell voltage required: 3.1 V at 100 mA cm^2, as opposed to 3.3 V required when paired with conventional OER (Fig. 1c). The decline in the FE of the E-to-EG conversion and a consequent increase in cell voltage after 2 h of operation was ascribed to the partial further oxidation of accumulated EG extended electrolysis (Fig. S13) and a partial migration or deposition of the Ru–POM complex (Fig. S15), as seen in a darkening of the Nafion membrane on the anodic side. On the cathodic side,

the NiSAC catalyst exhibited good stability under acidic CO$_2$R conditions with added KCl, retaining its original structure without Ni sintering or dissolution, as seen in post-reaction HR-TEM, XAS (Fig. S16 and S17), and inductively coupled plasma mass spectrometry of the electrolyte (Table S1).

To study the economic potential, we carried out a technoeconomic analysis (TEA) (Fig. 4c). When the market price of CO is $600 per ton and the value of EG is $800 per ton,[37] the CO$_2$R/OER in an acidic system sees a $200 deficit per ton of CO generated due to the high voltage required for this reaction pair and low product value. By changing the anodic reaction to an E-to-EG conversion, a lowering of voltage of 0.2 V leads to an $80 reduction in electricity, capital and operating related cost per
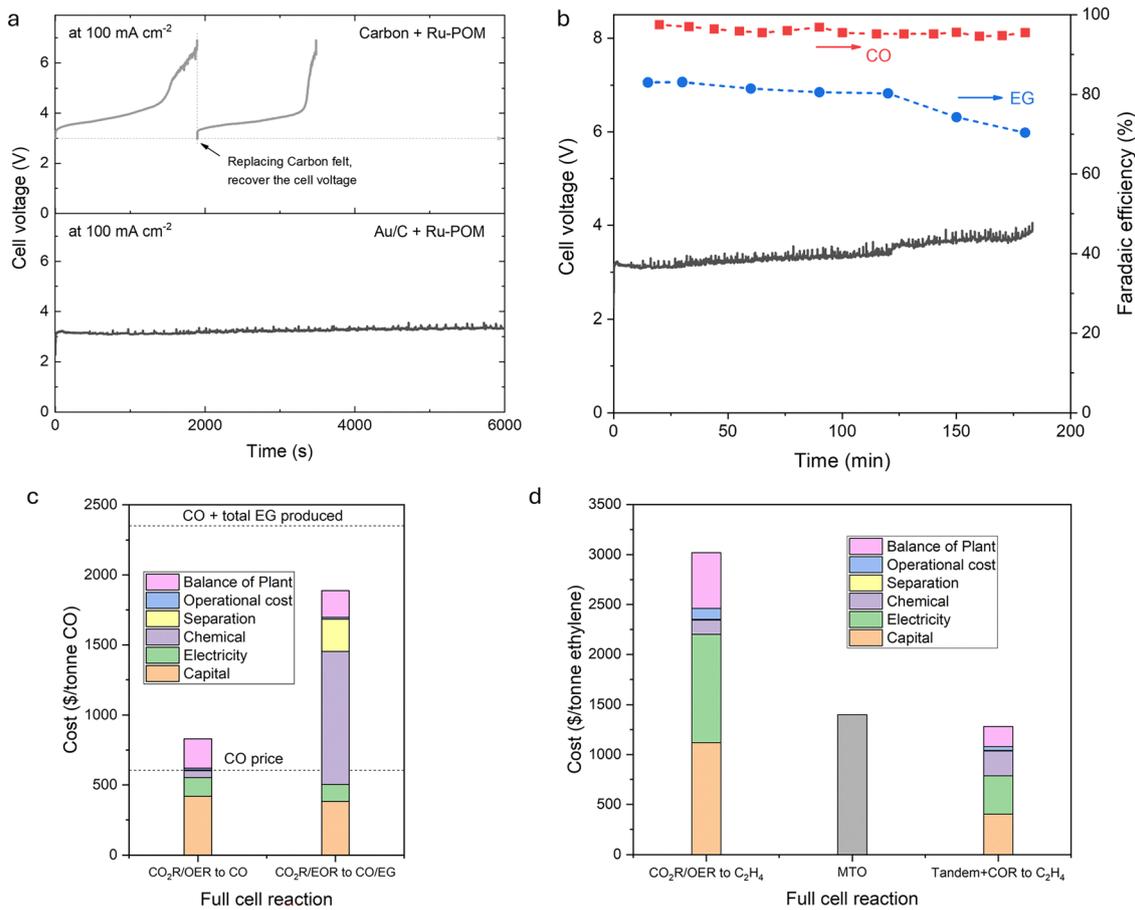
8604 | *Energy Environ. Sci.*, 2025, **18**, 8600–8607

This journal is © The Royal Society of Chemistry 2025

Fig. 4 Cell voltages (black) at 100 mA cm^{-2} for acidic CO_2-to-CO paired with optimized Ru–POM mediated ethylene oxidation to EG (a) in the first 6000 seconds for comparing the stability between Au/C and bare C felt as anodic electrodes and (b) for a longer period. Their faradaic efficiencies (right Y-axis) for CO_2-to-CO conversion (in red) and E-to-EG conversion (blue) are also plotted in (b). Technoeconomic analysis to compare the cost (c) from CO_2R/OER to CO and the CO_2R/ethylene oxidation reaction (EOR) to CO/EG, and (d) the ethylene production cost *via* the acidic CO_2R/OER pair and tandem CO_2R/EOR to CO followed by COR to ethylene; the methanol-to-olefin (MTO) process is listed for comparison.

ton of CO produced. The increase in the input chemical cost and separation cost is due to the usage of ethylene ($1000 per ton) as the reactant, and the distillation capital and operation for EG separation. However, the overall benefit coming from producing EG covers all of the increased cost in the chemical and separation, and leads to around $500 profit per ton of CO generated at the cathode.

In addition, we compared the ethylene production cost *via* acidic CO_2R/OER pair[38] and tandem CO_2R/ethylene oxidation reaction (EOR) to CO, followed by COR to ethylene (Fig. 4d).[39,40] By using a lower-cost estimate for CO produced through a tandem, ethylene is produced at a lower cost compared to direct CO_2R/OER in an acidic system and the methanol-to-olefin (MTO) process.[41] A lower cost of CO reactant is facilitated by CO_2R/EOR paired electrolysis, the lower full cell voltage and higher FE advantage of alkaline COR[39,40] compared to acidic CO_2R.[38]

Conclusions

In summary, we demonstrated the paired electrolysis combining acidic C_2H_4-to-EG conversion with acidic CO_2-to-CO

reaction. A homogeneous Ru–POM mediator was electrooxidized at the anode, and in turn, this oxidized ethylene *via* the redox cycle associated with its metal oxo species. The NiSAC catalyst facilitates high FE for the CO_2-to-CO conversion at the cathode. The full cell voltage of 3.1 V is below that needed in an OER-paired system. The choice of the Ru–POM oxidizing catalyst is important, with Au developing the intermediates required for this purpose, but suppressing O_2 evolution.

Author contributions

H. C., K. X., A. H.-B. and E. H. S. supervised the project. H. C. and H. S. performed the electrochemical measurements, materials synthesis, and characterization. They plotted the figures and wrote the manuscript. H. L. conducted SEM characterization and suggested the use of a NiSAC catalyst. R. K. M. supervised the measurement of the CO_2-to-CO cathodic reaction and its evaluation. R. X. & W. N. assisted in the design of the paired system and the result discussions. J. Y. supervised the redox-mediated electrocatalysis process, assisted in the synthesis of Ru–POM and the evaluation of E-to-EG. Y. L. supervised the measurement

This journal is © The Royal Society of Chemistry 2025

Energy Environ. Sci., 2025, **18**, 8600–8607 | **8605**

of the single pass conversion. B. P. & Y.C. contributed to the deposition of the metal layer electrode using the sputtering method. J. E. H and G. S carried out TEA. All authors discussed the results, and contributed to the writing and editing of the manuscript. K. X, E. H. S. and A. H.-B. revised the manuscript.

Conflicts of interest

There are no conflicts to declare.

Data availability

The data supporting this article have been included as part of the SI, and all of the original data can be obtained from the corresponding authors upon reasonable request. Supplementary methods, figures (Fig. S1–S17), table (Table S1), and references are available. See DOI: https://doi.org/10.1039/d5ee02847g

Acknowledgements

References

1 A. Ozden, F. P. García de Arquer, J. E. Huang, J. Wicks, J. Sisler, R. K. Miao, C. P. O'Brien, G. Lee, X. Wang, A. H. Ip, E. H. Sargent and D. Sinton, *Nat. Sustain.*, 2022, **5**, 563–573.

2 X. Sheng, W. Ge, H. Jiang and C. Li, *Adv. Mater.*, 2022, **34**, 2201295.

3 Y. Xie, P. Ou, X. Wang, Z. Xu, Y. C. Li, Z. Wang, J. E. Huang, J. Wicks, C. McCallum, N. Wang, Y. Wang, T. Chen, B. T. W. Lo, D. Sinton, J. C. Yu, Y. Wang and E. H. Sargent, *Nat. Catal.*, 2022, **5**, 564–570.

4 M. Fan, J. E. Huang, R. K. Miao, Y. Mao, P. Ou, F. Li, X.-Y. Li, Y. Cao, Z. Zhang, J. Zhang, Y. Yan, A. Ozden, W. Ni, Y. Wang, Y. Zhao, Z. Chen, B. Khatir, C. P. O'Brien, Y. Xu, Y. C. Xiao, G. I. N. Waterhouse, K. Golovin, Z. Wang, E. H. Sargent and D. Sinton, *Nat. Catal.*, 2023, **6**, 763–772.

5 J. Gu, S. Liu, W. Ni, W. Ren, S. Haussener and X. Hu, *Nat. Catal.*, 2022, **5**, 268–276.

6 J. E. Huang, F. Li, A. Ozden, A. Sedighian Rasouli, F. P. García de Arquer, S. Liu, S. Zhang, M. Luo, X. Wang, Y. Lum, Y. Xu, K. Bertens, R. K. Miao, C.-T. Dinh, D. Sinton and E. H. Sargent, *Science*, 2021, **372**, 1074–1078.

7 S. Verma, S. Lu and P. J. A. Kenis, *Nat. Energy*, 2019, **4**, 466–474.

8 C. M. Gabardo, C. P. O'Brien, J. P. Edwards, C. McCallum, Y. Xu, C.-T. Dinh, J. Li, E. H. Sargent and D. Sinton, *Joule*, 2019, **3**, 2777–2791.

9 H. Yadegari, A. Ozden, T. Alkayyali, V. Soni, A. Thevenon, A. Rosas-Hernández, T. Agapie, J. C. Peters, E. H. Sargent and D. Sinton, *ACS Energy Lett.*, 2021, **6**, 3538–3544.

10 A. Kormányos, A. Szirmai, B. Endrődi and C. Janáky, *ACS Catal.*, 2024, **14**, 6503–6512.

11 X. Wang, P. Li, J. Tam, J. Y. Howe, C. P. O'Brien, A. Sedighian Rasouli, R. K. Miao, Y. Liu, A. Ozden, K. Xie, J. Wu, D. Sinton and E. H. Sargent, *Nat. Sustain.*, 2024, **7**, 931–937.

12 M. S. E. Houache, R. Safari, U. O. Nwabara, T. Rafaïdeen, G. A. Botton, P. J. A. Kenis, S. Baranton, C. Coutanceau and E. A. Baranova, *ACS Appl. Energy Mater.*, 2020, **3**, 8725–8738.

13 R. Xia, R. Wang, B. Hasa, A. Lee, Y. Liu, X. Ma and F. Jiao, *Nat. Commun.*, 2023, **14**, 4570.

14 H. Yue, Y. Zhao, X. Ma and J. Gong, *Chem. Soc. Rev.*, 2012, **41**, 4218–4244.

15 Y. Lum, J. E. Huang, Z. Wang, M. Luo, D.-H. Nam, W. R. Leow, B. Chen, J. Wicks, Y. C. Li, Y. Wang, C.-T. Dinh, J. Li, T.-T. Zhuang, F. Li, T.-K. Sham, D. Sinton and E. H. Sargent, *Nat. Catal.*, 2020, **3**, 14–22.

16 C. Lucky, T. Wang and M. Schreier, *ACS Energy Lett.*, 2022, **7**, 1316–1321.

17 W. R. Leow, Y. Lum, A. Ozden, Y. Wang, D.-H. Nam, B. Chen, J. Wicks, T.-T. Zhuang, F. Li, D. Sinton and E. H. Sargent, *Science*, 2020, **368**, 1228–1233.

18 L. Huang, P. Wang, Y. Jiang, K. Davey, Y. Zheng and S.-Z. Qiao, *J. Am. Chem. Soc.*, 2023, **145**, 15565–15571.

19 M. Chung, K. Jin, J. S. Zeng and K. Manthiram, *ACS Catal.*, 2020, **10**, 14015–14023.

20 L. Fan, Y. Zhao, L. Chen, J. Chen, J. Chen, H. Yang, Y. Xiao, T. Zhang, J. Chen and L. Wang, *Nat. Catal.*, 2023, **6**, 585–595.

21 M.-H. Guan, L.-Y. Dong, T. Wu, W.-C. Li, G.-P. Hao and A.-H. Lu, *Angew. Chem., Int. Ed.*, 2023, **62**, e202302466.

22 S.-K. Zhang, Y. Feng, A. Elgazzar, Y. Xia, C. Qiu, Z. Adler, C. Sellers and H. Wang, *Joule*, 2023, **7**, 1887–1901.

23 A.-Z. Li, X. Wang, S. Li, B.-J. Yuan, X. Wang, R.-P. Li, L. Zhang, B.-J. Li and H. Duan, *J. Am. Chem. Soc.*, 2025, **147**, 10493–10503.

24 A.-Z. Li, B.-J. Yuan, M. Xu, Y. Wang, C. Zhang, X. Wang, X. Wang, J. Li, L. Zheng, B.-J. Li and H. Duan, *J. Am. Chem. Soc.*, 2024, **146**, 5622–5633.

25 J. H. Kim, H. Jang, G. Bak, W. Choi, H. Yun, E. Lee, D. Kim, J. Kim, S. Y. Lee and Y. J. Hwang, *Energy Environ. Sci.*, 2022, **15**, 4301–4312.

26 H. Zhang, S. Hwang, M. Wang, Z. Feng, S. Karakalos, L. Luo, Z. Qiao, X. Xie, C. Wang, D. Su, Y. Shao and G. Wu, *J. Am. Chem. Soc.*, 2017, **139**, 14143–14149.

27 T. Haas, R. Krause, R. Weber, M. Demler and G. Schmid, *Nat. Catal.*, 2018, **1**, 32–39.

28 R. B. Kutz, Q. Chen, H. Yang, S. D. Sajjad, Z. Liu and I. R. Masel, *Energy Technol.*, 2017, **5**, 929–936.

29 C. M. Tourné, G. F. Tourné, S. A. Malik and T. J. R. Weakley, *J. Inorg. Nucl. Chem.*, 1970, **32**, 3875–3890.

30 R. Neumann and M. Dahan, *Nature*, 1997, **388**, 353–355.

31 A. Sartorel, M. Carraro, G. Scorrano, R. D. Zorzi, S. Geremia, N. D. McDaniel, S. Bernhard and M. Bonchio, *J. Am. Chem. Soc.*, 2008, **130**, 5006–5007.

8606 | *Energy Environ. Sci.*, 2025, **18**, 8600–8607

This journal is © The Royal Society of Chemistry 2025

32 C. Casadevall, V. Martin-Diaconescu, W. R. Browne, S. Fernández, F. Franco, N. Cabello, J. Benet-Buchholz, B. Lassalle-Kaiser and J. Lloret-Fillol, *Nat. Chem.*, 2021, **13**, 800–804.

33 J. Yu, C. B. Musgrave, III, Q. Chen, Y. Yang, C. Tian, X. Hu, G. Su, H. Shin, W. Ni, X. Chen, P. Ou, Y. Liu, N. M. Schweitzer, D. M. Meira, V. P. Dravid, W. A. Goddard, III, K. Xie and E. H. Sargent, *J. Am. Chem. Soc.*, 2024, **146**, 32660–32669.

34 R. Neumann and C. Abu-Gnim, *J. Am. Chem. Soc.*, 1990, **112**, 6025–6031.

35 H. S. Lee, H. Shin, S. Park, J. Kim, E. Jung, W. Hwang, B.-H. Lee, J. M. Yoo, W. H. Antink, K. Lee, S. Lee, G. Na, K. Suh, Y. S. Kim, K.-S. Lee, S. J. Yoo, Y.-E. Sung and T. Hyeon, *Joule*, 2023, **7**, 1902–1919.

36 C.-Y. Li, J.-C. Dong, X. Jin, S. Chen, R. Panneerselvam, A. V. Rudnev, Z.-L. Yang, J.-F. Li, T. Wandlowski and Z.-Q. Tian, *J. Am. Chem. Soc.*, 2015, **137**, 7648–7651.

37 https://www.chemanalyst.com/Pricing/Pricingoverview.

38 Y. Chen, X.-Y. Li, Z. Chen, A. Ozden, J. E. Huang, P. Ou, J. Dong, J. Zhang, C. Tian, B.-H. Lee, X. Wang, S. Liu, Q. Qu, S. Wang, Y. Xu, R. K. Miao, Y. Zhao, Y. Liu, C. Qiu, J. Abed, H. Liu, H. Shin, D. Wang, Y. Li, D. Sinton and E. H. Sargent, *Nat. Nanotechnol.*, 2024, **19**, 311–318.

39 H. Wu, L. Huang, J. Timoshenko, K. Qi, W. Wang, J. Liu, Y. Zhang, S. Yang, E. Petit, V. Flaud, J. Li, C. Salameh, P. Miele, L. Lajaunie, B. Roldán Cuenya, D. Rao and D. Voiry, *Nat. Energy*, 2024, **9**, 422–433.

40 Y. Liang, F. Li, R. K. Miao, S. Hu, W. Ni, S. Zhang, Y. Liu, Y. Bai, H. Wan, P. Ou, X.-Y. Li, N. Wang, S. Park, F. Li, J. Zeng, D. Sinton and E. H. Sargent, *Nat. Synth.*, 2024, **3**, 1104–1112.

41 P. Hirunsit, A. Senocrate, C. E. Gómez-Camacho and F. Kiefer, *ACS Sustain. Chem. Eng.*, 2024, **12**, 12143–12160.

This journal is © The Royal Society of Chemistry 2025

Energy Environ. Sci., 2025, **18**, 8600–8607 | **8607**